Hemispheric Asymmetry of Sulcus-Function Correspondence: Quantization and Developmental Implications

Mohammed K. Hasnain,[1]* Peter T. Fox,[2] and Marty G. Woldorff[3]

[1]*NeuroCare of Southern Indiana, New Albany, Indiana*
[2]*Research Imaging Center, The University of Texas Health Science Center at San Antonio, San Antonio, Texas*
[3]*Center for Cognitive Neuroscience, Duke University, Durham, North Carolina*

Abstract: Spatial covariances between the geometric centers of human occipital sulci and visual functional areas were calculated to reduce the spatial variance of functional-area locations between subjects. Seven visual areas in each occipital hemisphere were retinotopically mapped, using horizontal- and vertical-meridian stimuli and ^{15}O PET in 11 subjects. Sulcal locations were determined using anatomic brain models derived from high-resolution MRI images. Location variability for sulci and functional areas was similar in magnitude, with average standard deviations of (2.7x, 5.3y, 5.7z) mm and (4.3x, 5.4y, 5.3z) mm, respectively. Sulcal locations were predictive of functional-area locations (i.e., significant spatial covariance) in the minority of structure-function pairings tested (25 of 168). Location variability was reduced by an average of 27% for functional areas showing significant covariation with sulcal features. Early-developing sulci were stronger predictors of functional-area location than late-developing sulci. Sulcus-function covariance was stronger in the left occipital lobe than in the right occipital lobe. Notably, the left calcarine fissure demonstrated powerful covariances with functional areas in both hemispheres, suggesting that it serves as a developmental "anchor" for functional areas in the occipital cortex. These findings support the hypothesis that hemispheric lateralization of function is reflected in the strength of correspondence between cortical surface anatomy and function. *Hum Brain Mapp 27:277–287, 2006.*

Key words: corticogenesis; handedness; lateralization; striate; extrastriate

INTRODUCTION

The first objective of our study was to test theories of neocortical development and hemispheric specialization. Careful characterization of the sulcal-functional covariance (or lack thereof) is valuable in choosing between theories of cortical development. In addition, theories on the biological foundations of hemispheric specialization propose that lateralization of function between hemispheres is mirrored in anatomic structure. Several developmental theories relating sulcation to the functional map have been put forward. These theories range from the theory of gyrogenesis as proposed by Welker [1990] and the tension-based theory of morphogenesis by Van Essen et al. [1997] on the one hand, to the mechanical folding hypothesis by Richman et al. [1975] on the other. These theories differ markedly in terms

Contract grant sponsor: Research Imaging Center; Contract grant sponsor: Human Brain Project; Contract grant number: P0I MH/DA52176.

Performed at the Research Imaging Center, The University of Texas Health Science Center at San Antonio.

*Correspondence to: Mohammed K. Hasnain, NeuroCare of Southern Indiana, PSC, 3605 Northgate Court, Suite 209, New Albany, IN 47150. E-mail: hasnain@earthlink.net

Received for publication 16 January 2005; Accepted 9 May 2005

DOI: 10.1002/hbm.20183

Published online 9 August 2005 in Wiley InterScience (www.interscience.wiley.com).

of the predictions that they make about sulcal-functional relationship and the mechanisms involved. This is a rather profound reflection of the lack of consistent data on sulcal-functional relationships from which theories can be derived. Furthermore, differential pattern in the strength of sulcus-function covariances between hemispheres would imply that hemispheric specialization manifests as hemispheric asymmetry in the structure-function correspondence.

The second objective of our study was to determine whether and to what degree spatial covariance between sulci and functional areas could be used to improve spatial normalization methods. Spatial normalization [Fox et al., 1985; Fox, 1995] is widely used to facilitate automated detection of functional areas and of structural abnormalities. As generally applied, global spatial normalization corrects for intersubject differences in brain dimensions and shape, but not for fine anatomical details, such as sulcal patterns. However, image morphing algorithms are now becoming available which can incorporate anatomical details, warping brains to one another with greater anatomical precision [Bilir et al., 1998; Woods et al., 1998; Ashburner et al., 1999; Green et al., 1999; Kochunov et al., 2000]. While the hope is that such anatomically precise intersubject registration will bring about similarly precise alignment of brain functional areas, these algorithmic advances will enhance the power of functional brain mapping only if (and to the degree that) reliable spatial covariances exist between surface features and functional areas. We have previously reported on structural-functional relationships in the human occipital lobe [Hasnain et al., 2001]. Here we extend that analysis further to explicitly calculate the sulcal contribution to location variance of functional areas after normalization to a common space by a nine-parameter affine transform and discuss the results in the context of theories of corticogenesis and cerebral lateralization.

SUBJECTS AND METHODS

Each of the early visual functional areas V1, V2v, V2d, VP, V3, and V3a contain a retinotopic map [Horton and Hoyt, 1991; Sereno et al., 1995]. These areas lay out on the occipital cortex in a continuous manner, beginning with V1 and moving inferior (V2v, VP, V4v) and superior (V2d, V3, V3a) along an axis running dorsal-ventral to V1. Functional area borders alternate between their horizontal-meridian (HM) and vertical-meridian (VM) representations. Exploiting this organizational property, we used meridian-stimuli to define functional-area centers and borders. Functional activations were detected by $H_2{}^{15}O$ PET. Models of the occipital-lobe cortical surface were made for each subject, using high-resolution (1 mm^3) MRI images. The datasets were coregistered and transformed into a common space to compute spatial variability and spatial covariance [Talairach and Tournoux, 1988; Lancaster et al., 1995]. Where significant covariance was found ($r > 0.6$ in 2 or more axes) between a sulcus and a functional area, a correction vector was computed from the sulcal locations and applied to the functional area locations. The reduction in functional-area spatial variability achieved by the sulcal-location correction represents the fraction of total variance due to surface anatomy.

Subjects

A total of 11 normal right-handed men between the ages of 18 and 35 years were recruited after informed consent was obtained as approved by the institutional review board of the University of Texas Health Science Center at San Antonio. Handedness restriction was used to avoid confounds due to differences in hemispheric anatomy between left- and right-handed subjects and was determined by a standard questionnaire regarding hand usage. A medical history battery questioned the subjects about neurological, psychiatric, and cardiovascular history.

MRI Data Acquisition and Cortical Surface Modeling

To acquire the anatomic data, the subjects underwent a T_1-weighted MRI brain scan in a 1.9 T Elscint Prestige; voxel size = 1 mm^3; matrix size = $256 \times 192 \times 192$. A moldable facemask system was used to minimize motion during scanning. The scalp and the skull were removed from the images, which were then normalized into Talairach space using the Lancaster algorithm [Talairach and Tournoux, 1988; Lancaster et al., 1995]. The MRX software package (GE Research and Development Laboratory, Schenectady, NY) was used to create models of the cortical surface from the normalized MRI dataset for each subject.

Labeling of Occipital Sulci

Sulcal designations were based on order and orientation with respect to the calcarine sulcus as visualized on the cortical surface models. The calcarine sulcus was easily defined as the only major sulcus extending from the occipital pole to the junction with the parieto-occipital sulcus (Fig. 1a). Starting from the occipital pole, the first and the second sulci immediately dorsal to the calcarine with their origins on the posterior surface of the brain were marked. These were labeled the "first dorsal sulcus" and the "second dorsal sulcus," respectively. Similarly, starting from the occipital pole, the first and the second sulci immediately ventral to the calcarine with their origins on the inferior surface of the brain were identified and labeled the "first ventral sulcus" and the "second ventral sulcus," respectively. Sulci confined to the medial surface without extension to the posterior or inferior surface were excluded. The collateral sulcus was identified using a standard atlas as a guide [Ono et al., 1990]. This sulcus was usually the only sulcus starting from the inferior-medial surface of the occipital lobe and extending midway into the temporal lobe. Independent observers were asked to cross-validate when there was any doubt in designation. In cases where the occipital limb of the collateral sulcus also happened to be the first or the second ventral sulcus, the sulcus was given both designations and counted in the analysis for both sets of sulci. Similar to the concept of center-of-mass of activation in PET data, the geometric cen-

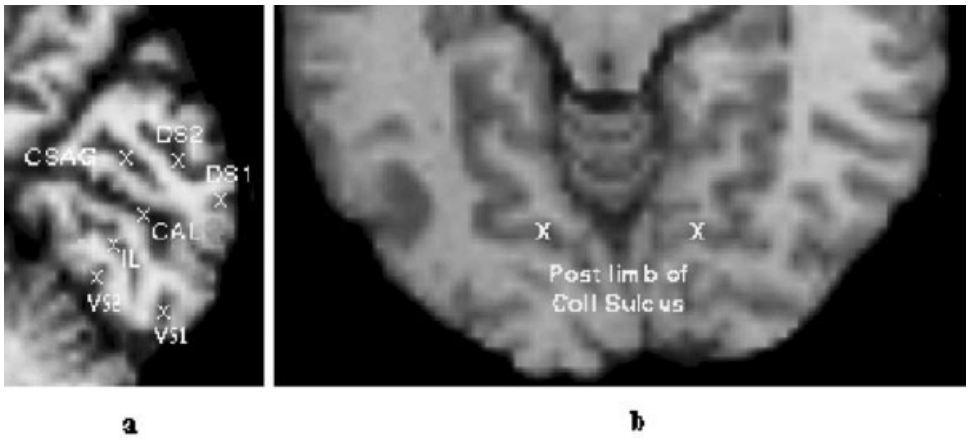

Figure 1.

Selected sulcal landmarks, **a:** Sagittal MRI view of the brain illustrating relative locations of medial occipital sulci identified in the study. CAL, calcarine sulcus; DS1, first dorsal sulcus; DS2, second dorsal sulcus; VS1, first ventral sulcus; VS2, second ventral sulcus; IL, intralingual sulcus; CSAG, cuneosagittal sulcus. The last two sulci were found only in four left and six right hemispheres, respectively, and thus were not included in the analysis. **b:** Axial view of the brain showing the collateral sulcus (Coll). X marks the center of the occipital limb of the collateral sulcus.

ter of a sulcus was used as the reference point for that sulcus in correlation analysis. The center of the sulcus was calculated using 3D models generated by the MRX software package (GE) and confirmed by localization in axial, coronal, and sagittal slices viewed simultaneously using the Lancaster algorithm [Talairach and Tournoux, 1988; Lancaster et al., 1995]. For the collateral sulcus, the center of its occipital limb was taken as the reference point (Fig. 1b).

Experimental Tasks

Subjects were scanned under three experimental settings: fixation point (FIX), random dots along the horizontal-meridian (HM), and random dots along the vertical-meridian (VM) (Fig. 2). Nine scans were acquired for the three test conditions in the sequence: FIX – HM – VM – FIX – VM – HM – FIX – HM – VM. In the FIX (control) condition, subjects viewed a crosshair with no other visual stimulation. In the HM and VM conditions (Fig. 2), subjects viewed sectors of random-dots patterns refreshing at a rate of 8 Hz to maximize response [Fox and Raichle, 1984]. Each stimulation field extended from 1° out to 18° eccentricity and spanned 60° of arc around the horizontal-meridian (HM condition), and around the vertical-meridian (VM condition), respectively.

PET Data Acquisition

We employed functional positron emission tomography (PET) to distinguish the borders between functional visual areas. $H_2{}^{15}O$ (half-life 123 s) was used as a freely diffusible blood-flow tracer, delivered via an intravenous bolus [Herscovitch et al., 1983; Raichle et al., 1983]. Data was acquired as regional distributions of tracer-associated radiation using a GE/Scanditronix 4096 PET camera with a spatial resolution of 5 mm (full-width at half-maximum) for events occur-

Figure 2.

Visual stimuli: still frames of random-dots pattern (50% density) stimuli. Subjects were scanned while observing either the horizontally or vertically oriented patterns to activate visual function area borders. The patterns refreshed at 8 Hz to maximize response intensity [Fox and Raichle, 1984]. In the control condition, subjects viewed a crosshair with no other visual stimulation.

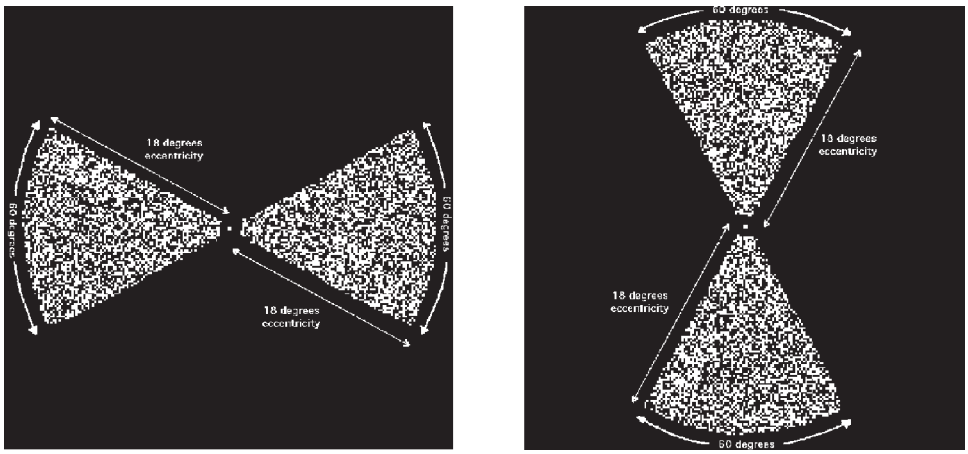

ring within each emission scan. Each scanning session consisted of one transmission scan (used for attenuation correction), followed by nine emission scans (separated by 11 min to allow radiodecay), three for each of the three experimental conditions. Interscan head motions were removed using a modified version of the AIR algorithm [Woods et al., 1993]. The dimensions of a particular individual's brain along the three axes were derived from the MRI data, and then the same scaling factors were used to normalize both functional and anatomic images into Talairach space [Talairach and Tournoux, 1988; Lancaster et al., 1995]. The resulting brain contours in the PET and MRI datasets were coregistered within 2 mm of each other in each of the three axes. The three images in each condition were averaged and then contrasted on a voxel-wise basis, creating per-subject statistical parametric images (SPI) of task-induced changes in regional blood flow for each of the two stimulus conditions (HM and VM) relative to the control state (FIX). For each SPI an automated search for local maxima and minima was performed using a search volume measuring 27 mm^3. A maxima was identified as being greater than its 26 neighbors. The output of the local maximum search is the change distribution across the brain volume. Change distribution analysis (CDA) [Fox et al., 1988] was used to assess the statistical significance of the identified outliers. CDA identifies physiological responses as outliers in the noise distribution by using a one-sided gamma-2, a modification of the conventional outlier detection statistic [Fox et al., 1988]. SPIs were converted to z-score images, based on the aggregate variance of all local changes within each nine-image set for each subject. Extrema with z-scores > 1.96 were considered significant.

Labeling of Local Maxima as Functional Borders

Labeling of functional areas was performed by superimposition of regional functional activations as detected by PET-derived z-score images, on the surface models for the occipital lobes, and by following the cortical surface along a dorsal-ventral axis from the V1 horizontal-meridian (HM) representation. The calcarine sulcus has been established as the site of the HM representation in the primary visual cortex (V1) of man. Therefore, the HM activation in V1 (V1(H)) was recognized by reference to the calcarine sulcus. Visual area borders were identifiable as alternating bands of activations due to the vertical and horizontal meridian stimuli extending out from the calcarine. The coordinates for the geometric center of a visual area were obtained by averaging those for its borders, e.g., the center of V2v was obtained by averaging the coordinates for its borders V1/V2v and V2v/VP (Fig. 3). For the "color-sensitive" area (V4v), a directed local-maximum search strategy was performed because the retinotopy in this area is not well defined [for details, see Hasnain et al., 1998].

SULCAL–FUNCTIONAL SPATIAL COVARIANCE

All data were transformed into a common space to compute spatial variability and spatial covariance [Talairach and Tournoux, 1988; Lancaster et al., 1995]. The sulci and functional areas were reduced to their respective approximate geometric centers in order to compute the correlation "r" statistic. Pair-wise correlation analysis was carried out for each of the selected areas and sulci within each hemisphere. Given the large number of sulcal-area pairs compared in each hemisphere (84), we calculated the probability of making a type I error in our analysis. If we assume that some of the statistically significant correlations were due to chance alone, it follows that these *randomly* occurring "significant" correlations in the three axes would be independent of each other. Therefore, we can apply the multiplication rule of probabilities. Since there are three possible combinations for each pair (x-x and y-y covariance, x-x and z-z covariance, y-y and z-z covariance), the odds of a sulcus-functional area pair having significant correlations in at least two of the three axes by chance alone is 3 in 400 or 1 in 133 ($P < 0.0075$). An area was therefore considered to significantly covary with a sulcus only if the pair had positive spatial correlations with a $P < 0.05$ ($r = 0.6$ for a sample size of 11) in at least two axes.

If a sulcus and a functional area covary across a population, it follows that, in general, the displacement of one from its mean will predict the displacement of the other from its mean in a given individual. Thus, if S^2 is the sample variance (sample size n) of a functional area in a stereotaxic space in a particular axis, such that:

$$S^2 = \frac{\sum (X_m - X_I)^2}{n-1}$$

(X_m = mean location for that functional area, X_I = location of the functional area in an individual), then this variance can be reduced (to S_c^2) by subtracting a correctional vector C_i (based on a covarying sulcus), from the location X_i for that functional area in each of the individuals, as follows:

$$S_c^2 = \frac{\sum (X_m - (X_I - C_I))^2}{n-1}$$

where the correctional vector C_i is the displacement of the center of the covarying sulcus in a subject (s_I) from the sample mean for that sulcus (s_m) in a given axis ($C_i = s_i - s_m$). We calculated these correctional vectors in each individual for sulci that were found to have significant covariances with a particular area in at least two of the three cardinal axes and applied these vectors to reduce the area's location variance (Fig. 4).

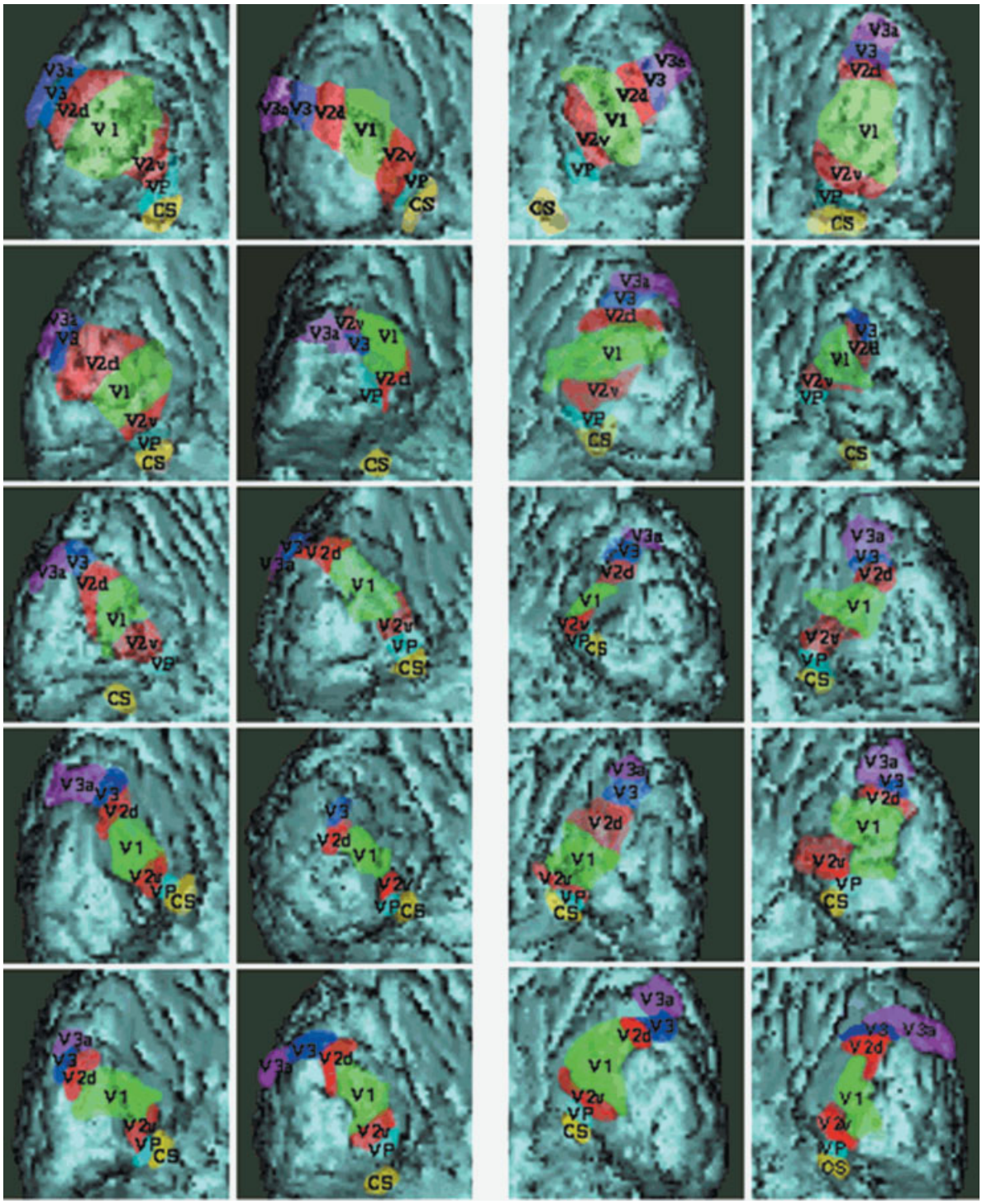

Figure 3.
Cortical surface models of early visual areas: posteromedial views of left and right occipital lobes of 10 subjects illustrating the relative positions of the early visual areas. Area locations and shapes are approximate due to the folded sulci of the brain model.

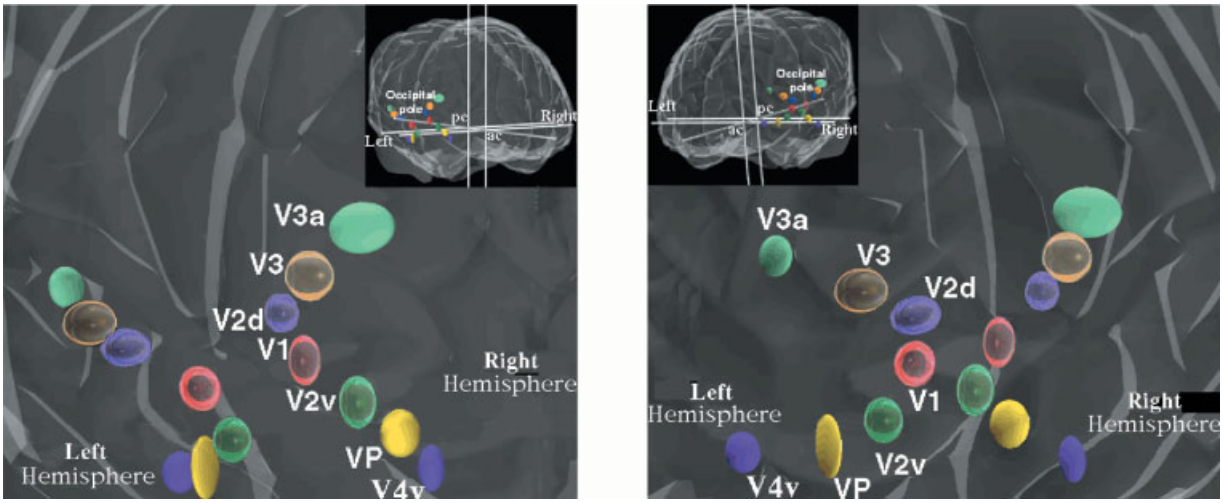

Figure 4.

3D sample-based brain models illustrating sulcal-functional covariance: Transparent ellipsoids centered at the mean location of respective functional visual areas represent variance of functional areas in Talairach space before sulcus-based reduction. Solid ellipsoids within each transparent ellipsoid represent variance of functional areas in Talairach space after sulcus based reduction. ac, anterior commissure; pc, posterior commissure. All reductions are based on the left calcarine except for area V3. Right area V3 correction is based on the right calcarine and in the left hemisphere it is based on the second ventral sulcus.

RESULTS

Sulcal-Functional Covariances

One sulcus-functional area covariance matrix of 6 * 7 * 3 members was constructed for each half of the two occipital lobes (superior and inferior to the calcarine sulcus). Thus, four matrices were constructed representing the four visual field quadrants. The entries of the matrices were covariances of six sulci with seven functional areas in each of the three axes (x, y, z), making a total of 504 correlations tested. For this number of correlations and at a *P*-value of 0.05, chance alone would predict 25 single-axis correlations, four two-axis correlations, and no (fewer than 0.05) three-axis correlations. These expectations were greatly exceeded: 130 single-axis correlations (89 on the left; 41 on the right); 23 two-axis correlations (14 on the left, nine on the right); two three-axis correlations (both on the left), indicating that the findings could not be explained by chance alone. Further analysis was carried out on the subset of two-axis and three-axis correlations, as listed in Table I.

Structure-function covariances were more frequent and generally stronger in the left hemisphere (16) than in the right hemisphere (9), suggesting tighter structure-function correspondence in the left occipital lobe than in the right. Not unexpectedly, the calcarine sulci accounted for the greatest number of significant covariances: 9 of 25. These occurred, however, chiefly in the left hemisphere (6 of 9), again suggesting a left-hemisphere "dominance" in structure-function correspondence. Notably, variations in calcarine location predicted not only V1 location variances, but also location variances for V2 and V3, both dorsal and ventral. This suggests that if in a given subject the calcarine lies more superior (or inferior) than the average, then the entire ensemble of functional areas will be shifted accordingly.

Following calcarine, the second ventral and second dorsal sulci were the most reliably predictive of functional area spatial variability, accounting for 8 and 5 covariances, respectively. Area VP and area V4v were closely associated with the occipital limb of the collateral sulcus such that area VP was usually found at the medial lip, and area V4v was found within the confines of the occipital limb of the collateral sulcus (in 19 out of 22 subjects). For all sucli, the great majority of significant covariances were in the superior-inferior (z; n = 24) or anterior-posterior (y; n = 23) dimensions. Only five pairs showed x-axis covariance. This may be due to the fact that the sulci and areas in the medio-posterior occipital lobe are organized more or less along the z-axis and can be classified as being ventral (inferior) or dorsal (superior) to the primary visual cortex or the calcarine.

Folding patterns can be dramatically altered by prenatal lesions that perturb long-distance connections [Goldman-Rakic, 1980] and tension along axons in the white matter, including the corpus callosum, has been proposed as a possible mechanism causing the cortex to fold in a characteristic pattern [Van Essen, 1997]. To test this hypothesis, we examined interhemispheric covariances to assess if the location of sulcal landmarks in one hemisphere correlated with the location of functional area-centers in the opposite hemisphere. Two covariance matrices of 6 * 7 * 3 members were constructed: 6 sulci × 7 functional areas × 3 coordinates (x, y, z), for each hemisphere, making a total of 252 correlations

TABLE I. Areas and sulci with significant positive correlations in at least two axes and resultant decreases in location variability of functional areas

	Sulcal correlation coefficients			Reduced standard deviations (in mm) based on significant correlations (%)		
Area	x	y	z	x	y	z
Right hemisphere						
V1 (H): 2nd ventral sulcus	0.681	0.734	0.252	20.6 (−24%)	40.7 (−20%)	
V2d: Calcarine	0.246	0.648	0.648		30.9 (−10%)	40.2 (−7%)
V2d: 2nd dorsal sulcus	0.091	0.629	0.706		40.0 (−6%)	40.2 (−6%)
V3: Calcarine	0.042	0.707	0.718		40.0 (−27%)	30.7 (−11%)
V3/V3a: Calcarine	−0.074	0.724	0.611		40.6 (−31%)	40.4 (−2%)
V3/V3a: 2nd dorsal sulcus	−0.108	0.618	0.657		50.3 (−20%)	40.5 (1%)
V2v: 1st ventral sulcus	−0.297	0.657	0.679		40.6 (−23%)	40.9 (−16%)
V2v: 2nd ventral sulcus	0.260	0.755	0.663		40.5 (−24%)	40.5 (−24%)
V2v/VP: 2nd ventral sulcus	0.423	0.828	0.761		30.9 (−20%)	40.0 (−35%)
Left hemisphere						
V1: Calcarine	0.728	0.855	0.904	20.3 (−31%)	30.0 (−44%)*	30.5 (−53%)*
V1: 2nd dorsal sulcus	0.580	0.741	0.901		30.7 (−30%)	30.9 (−48%)*
V1(H): 2nd dorsal sulcus	0.376	0.828	0.835		20.4 (−43%)*	40.9 (−40%)
V1/V2d: Calcarine	0.616	0.875	0.873	40.9 (−18%)	50.2 (−34%)	50.9 (−41%)
V1/V2v: Calcarine	0.462	0.699	0.797		40.5 (−27%)	30.4 (−37%)
V2d: Calcarine	0.431	0.909	0.816	40.7 (−20%)	20.2 (−48%)*	50.3 (−38%)
V2d: 2nd ventral sulcus	−0.515	0.692	0.867		30.9 (−9%)	40.8 (−44%)*
V1/V2d: 1st ventral sulcus	0.608	0.436	0.780			60.9 (−30%)
V3: Calcarine	−0.121	0.679	0.698		30.8 (−25%)	50.4 (−28%)
V3: 2nd ventral sulcus	−0.671	0.639	0.843		40.4 (−12%)	40.2 (−45%)*
V2d/V3: 2nd ventral sulcus	−0.542	0.638	0.856		40.8 (−18%)	40.6 (−44%)*
V2v: Calcarine	0.501	0.833	0.838		30.0 (−42%)*	20.9 (−41%)
V2v: 2nd ventral sulcus	0.248	0.697	0.770		40.0 (−20%)	30.4 (−30%)
V1/V2v: 2nd dorsal sulcus	0.446	0.655	0.806		40.8 (−22%)	50.5 (+2%)
V2v/VP: 1st ventral sulcus	0.623	0.439	0.728	30.6 (−21%)	50.9 (−21%)	40.2 (−31%)
V2v/VP: 2nd ventral sulcus	0.077	0.619	0.816			30.6 (−42%)*

Significance is set at $P < 0.05$ in each axis.
In column 2, where a single functional area is named, the correlation is with the center of the area; where two functional areas are named (e.g., V1/V2v), the correlation is with the border between the two areas. Correlation coefficient (R) of 0.6 has a significance of $P < 0.05$ for n = 11.
* Statistically significant reduction in variance (>41%, using the *F*-test statistic, $P < 0.05$). x-axis = medial-lateral axis; y-axis = anterior-posterior axis; z-axis = superior-inferior axis.

tested. There were 40 single-axis correlations and six two-axis correlations. All two-axis correlations involved the left calcarine and the right second ventral sulcus (Table II). The left calcarine sulcus, in particular, covaried significantly with multiple areas in the contralateral hemisphere (Fig. 4), thus being a strong predictor of functional locations in both hemispheres.

Sulcal Contribution to Functional-Area Variability

Correction vectors were computed for the eight functional areas whose location was predicted by sulcal-functional covariance in at least two axes to test the fraction of the total spatial variance of functional areas that can be attributed to surface-feature location variance. On average, sulcal-location based corrections reduced functional-area variability by 1.6 mm, which was 27% of the average variability (5.9 mm SD) of the selected functional areas. The average reduction of variance in the left hemisphere (2.0 mm, 32%) was significantly greater ($P < 0.0001$) than that in the right hemisphere (0.9 mm, 17%). In addition, all corrections that lead to significant reductions in *individual* variances were based on sulcal features in the left hemisphere (Tables I, II, Fig. 4), again suggesting greater structure-function correspondence in the left hemisphere.

DISCUSSION

Sulcal-Function Covariance and Theories of Corticogenesis

A specific pattern of covariance between sulcal and functional anatomy has direct implications for evaluating theories of corticogenesis. There are three currently prevalent theories of sulcal and gyral development. The first theory, proposed by Richman et al. [1975], hypothesizes that sulci develop because of simple random mechanical buckling of cortical surface due to greater tangential growth rates of superficial cortical layers when compared to deeper cortical layers. For example, cortical areas with a greater surface area discrepancy between superficial and deeper layers also have more sulci [Armstrong et al., 1991, 1995]. This theory pre-

TABLE II. Interhemispheric correlations with significance in at least two axes and resultant decreases in location variability of functional areas

	Sulcal correlation coefficients			Reduced standard deviations (in mm) based on significant correlations (%)		
	x	y	z	x	y	z
Right 2nd ventral sulcus						
LV1: Right 2nd ventral sulcus	0.477	0.805	0.767	40.0 (−24%)		50.0 (−34%)
LV2v: Right 2nd ventral sulcus	0.078	0.731	0.811	40.6 (−9%)		20.9 (−41%)
Left calcarine						
RV1: Left calcarine	0.477	0.698	0.601	40.2 (−27%)		40.6 (−8%)
RV2v: Left calcarine	0.354	0.688	0.682	40.3 (−27%)		40.1 (−31%)
RV2d: Left calcarine	−0.201	0.892	0.656	20.0 (−54%)*		40.1 (−9%)
RV3: Left calcarine	−0.282	0.701	0.655	30.9 (−29%)		40.0 (−4%)

Significance is set at $P < 0.05$ in each axis.
Correlation coefficient (R) of 0.6 has a significance of $P < 0.05$ for n = 11.
* Statistically significant reduction in variance (>41%, using the *F*-test statistic, $P < 0.05$).

dicts a relative lack of covariance between sulci and functional areas. The second theory to explain gyrogenesis was proposed by Welker [1990], who observed that in ferret and raccoon brains the distance between sulcal pits and the ventricular surface did not increase as the cortex convoluted. Sulci in these animals divide the somatosensory cortex into areas representing specific body regions such as head from trunk, trunk from extremities, etc. [Smart and McSherry, 1986], thus predicting a strong correspondence of functional area borders with sulci. Finally, the tension-based theory of morphogenesis and compact wiring [Van Essen, 1997] proposes that the cortex folds in a characteristic pattern because of tension along axons in the white matter. This theory predicts that functional zones with strong connections should covary with sulcal pits such that the aggregate axonal length is minimized.

We found that although the primary sulci have a more consistent spatial relationship with neighboring functional areas, this did not hold true for secondary and tertiary sulci. No strict correspondence was found between gyral crowns and area centers or between sulci and functional borders. However, the three seemingly competing theories of cortical sulcation may actually be complementary, when considered to be differentially active during the various phases of corticogenesis. Formation of the primary sulci in mammals occurs in the second trimester, when predominantly glutamate-ergic pyramidal neurons migrate from the ventricular proliferative centers to the cortical surface traveling along glial radials [Rakic, 1990]. During this stage of radial growth of the cerebral cortex, the development of primary sulci and functional areas may be tightly linked, as witnessed by the relatively constant relationship between functional areas and the calcarine and the collateral sulci. During the third trimester and for some time after birth, cortical development is predominated by the maturation of the neuropil [Berry, 1982]. GABA-ergic interneurons originating from the lateral ganglionic eminence migrate tangentially during the third trimester [Anderson et al., 2001; Corbin et al., 2001]. Hence, tangential growth of the cerebral cortex continues after radial migration of neurons is complete. The tangential growth is greater in the outer cortical lamina as compared with the inner cortical layers [Richman et al., 1975; Armstrong et al., 1995]. This must occur after radial growth is complete, because the outer layers are the last to form during radial migration of neurons. Formation of secondary and tertiary sulci during the third trimester may be more influenced by simple mechanical folding of the cortex, which can actually distort the original shape and placement of the sulci and functional areas, thus accounting for a lower covariance of functional areas with secondary and tertiary sulci. Lastly, our finding of interhemispheric covariances may be due to tension along the axon bundles in the corpus callosum during the formation of interhemispheric connections, thus minimizing the aggregate length of axonal and dendritic wiring, as hypothesized by Van Essen [1997], and contributing directly to the compactness of neural circuitry.

Asymmetric Distribution of Structure–Function Covariances and Cerebral Dominance

As reported in the Results, there was considerable asymmetry between the two hemispheres in the magnitude and frequency of significant covariances (Table I). More sulcal-functional covariances were found in the left hemisphere. These covariances were generally stronger than those found in the right hemisphere, and all individually significant reductions in location variance of functional areas were due to corrections based on left hemispheric sulci. The left calcarine sulcus covaried significantly with areas in the ipsilateral as well as contralateral hemisphere, thus being a strong predictor of functional locations in both hemispheres.

Interhemispheric asymmetries of sulcal patterns and functional areas are well documented. These reports show a lower degree of variability in surface size and a stronger genetic influence on the size of several cortical surface areas in the left hemisphere [Tramo et al., 1995]. Sulcal variance in

the left posterior region was found to be less than that in the right posterior region, with deeper sulci being more comparable than superficial ones in right-handed monozygotic twins [Lohmann et al., 1999]. Other studies have shown a larger planum temporale, parietal and frontal operculum on the left, as well as a wider and longer left occipital lobe in right-handers [LeMay, 1977; Habib et al., 1995]. These differences extend to the cytoarchitectonic and molecular level, with longer axons and less neuronal density in the left Brodmann area 22 [Gazzaniga, 2000], and a larger left area TPT (part of Brodmann area 22) with greater cholineacetyltransferase activity than the right [Galaburda and Sanides, 1980; Amaducci et al., 1981]. Such anatomic and functional asymmetries between the hemispheres form the basis of the Geschwind and Galaburda [1985] theory of cerebral lateralization. This theory proposes that the developmental forces leading to interhemispheric asymmetry arise from a differential growth and maturation rate of functional areas due to a combination of genetic, hormonal, and environmental influences, and lead to a functional advantage for one hemisphere over the other for specific tasks.

These mechanisms cause microscopic as well as macroscopic interhemispheric asymmetry. For example, dendritic development in the vicinity of Broca's area on the left lags behind its homolog on the right, and sulcal patterns develop earlier on the right [Chi et al., 1977, Scheibel, 1984]. The macroscopic interhemispheric differences in surface area may be due to asymmetric postmigration cell loss [Galaburda et al., 1990], which occurs as intracortical connections are being formed. Sulcal pits exhibit the greatest degree of selective cell loss during this period, as the cortical surface undergoes a remolding with disappearance of some sulci formed during the second trimester and emergence of new and more permanent secondary sulci in the third trimester [Savel'ev, 1989]. The selective cell loss may be driven by hemispheric specialization via callosal connections [Rosen, 1996], as suggested by a relative lack of hemispheric asymmetry in individuals who are not left-hemisphere-dominant [Habib et al., 1995]. This is possible because selected neurons send axons across the corpus callosum even while they are migrating to the cortical surface during morphogenesis [Schwartz et al., 1991]. Our finding of interhemispheric sulcal-functional covariance supports the hypothesis that callosal connectivity plays a significant role in the genesis of cortical surface asymmetry, with functional areas and sulci in one hemisphere affecting the placement of structures in the other hemisphere. The left calcarine sulcus may serve as a developmental "anchor," influencing placement of not only the surrounding anatomic and functional structures, but also of homologous structures in the contralateral hemisphere, resulting in a decreased strength of sulcal-functional covariance intrinsic to the right hemisphere. A conclusive test of this hypothesis would be to repeat our study in strongly right-hemisphere-dominant individuals to see if the lateralization of sulcal-functional covariance disappears or reverses to the right hemisphere.

As addressed above, a specific pattern of covariance between sulcal and functional anatomy has direct implications for evaluating theories of corticogenesis. Since the asymmetric distribution of structure-function covariance could be an artifact of Talairach normalization and not truly morphologic, we compared the mean standard deviations in the x, y, and z-axes in both hemispheres using a factorial ANOVA design. Our analysis indicated that side (hemisphere) had no significant effect. We went to considerable lengths to analyze whether there was any difference in the ability of the Talairach space construct to reduce variability of functional areas in one hemisphere vs. another in our article in *Human Brain Mapping* [Hasnain et al., 1998]. No statistically significant difference was found when the mean standard deviations for x, y, and z axes in the left hemisphere were compared with their respective counterparts in the right hemisphere. Neither could any statistically significant difference be found between the pooled standard deviations across all axes in the left hemisphere (4.8 mm) vs. the pooled standard deviation across all axes in the right hemisphere (5.0 mm). For sulci, only the x-axis variance of left second dorsal sulcus was significantly different from its counterpart in the right hemisphere. Thus, the asymmetry of sulcal-functional covariance between hemispheres was evident, despite the symmetric reduction of variance of sulci and functional areas in the two hemispheres by normalization into Talairach space, and therefore independent of it [for a detailed analysis of functional and sulcal spatial variances, see Hasnain et al., 1998, 2001].

Applications to Spatial Normalization Algorithms

The second objective of our study was to test if sulcal-functional covariances can be used to explicitly reduce residual intersubject location variance of functional areas after nine-parameter global normalization (three each for rotation, translation, and scaling). Normalization techniques aim to reduce intersubject location variability of reported anatomic and functional structures, thereby allowing images from different individuals and research studies to be compared and combined, leading to better clinical prognostication and preoperative planning. The residual average location standard deviation of visual functional areas of our data was on the order of 5 mm in the stereotaxic space based on the atlas of Talairach and Tournoux [1988]. Other global techniques such as the convex hull (CH) method [Lancaster et al., 1999], where brain surfaces are selected as the basis for automating and standardizing spatial normalization, complement a nine-parameter normalization algorithm and further reduce variability. However, global spatial normalization methods cannot correct for smaller regional differences, as illustrated in Figure 3. Regional spatial normalization methods compute a 3D array (deformation field: DF) with 3D displacement vectors in each node [Collins et al., 1999; Kochunov et al., 1999], providing a mapping from points in the source brain to corresponding points in the target's volume space, or vice versa.

While the regional normalization techniques are capable of matching anatomic images with exceptional precision (approaching image resolution), it is largely unknown if selective or nonselective matching of detailed surface features of sulcal shape and size will lead to enhanced reduction in location variability of brain functional areas. We used the center-of-mass concept to assign reference values to sulci, thus simplifying the considerable variance in sulcal shape and size and providing a well-behaved location metric. We found that the approximate center-of-mass of specific sulci covaried with early visual functional areas in a 3D Cartesian construct, and the reductions in variability of functional areas based on these sulcal-functional covariances were significant (Tables I and II). These reductions reflect the fraction of location variance of functional areas that can be accounted for by sulcal variability. Thus, selected occipital sulcal landmarks contain information about functional topography, which provides search limits for localizing early visual functional areas and may be used to improve on linear normalization algorithms. Using our data, Kochunov et al. [2003] recently applied the Octree regional spatial normalization method to enhance statistical significance of intersubject activations over that achieved by global normalization of the data in the primary visual areas. Sulcal landmarks have also been used to enhance functional area matching between subjects by Fischl et al. [1999]. Our findings provide impetus for further studies quantifying and applying similar relationships in other areas of the brain.

ACKNOWLEDGMENTS

We thank B. Rowe for administrative support. We also thank J. Roby, B. Heyl, S. Mikiten, H. Downs, and P. Jerabek for valuable technical assistance.

REFERENCES

Amaducci L, Sorbi S, Albanese A, Gainotti G (1981): Choline acetyltransferase (ChAT) activity differs in right and left temporal lobes. Neurology 31:799–805.

Anderson SA, Marin O, Horn C, Jennings K, Rubenstein JL (2001): Distinct cortical migrations from medial and lateral ganglionic eminences. Development 128:353–563.

Armstrong E, Curtis M, Buxhoeveden DP, Fregoe C, Zilles K, Casanova MF, McCarthy WF (1991): Cortical gyrification in the rhesus monkey: a test of the mechanical folding hypothesis. Cereb Cortex 1:426–432.

Armstrong E, Schleicher A, Omran H, Curtis M, Zilles K (1995): The ontogeny of human gyrification. Cereb Cortex 5:56–63.

Ashburner J, Friston KJ (1999): Nonlinear spatial normalization using basis functions. Hum Brain Mapp 7:254–266.

Berry M (1982): Cellular differentiation: development of dendritic arborizations under normal and experimentally altered conditions. Neurosci Res Prgm Bull 20:451–461.

Bilir E, Craven W, Hugg J, Gilliam F, Martin R, Faught E, Kuzniecky R (1998): Volumetric MRI of the limbic system: anatomic determinants. Neuroradiology 40:138–144.

Chi JG, Dooling EC, Gilles FH (1977): Gyral development of the human brain. Ann Neurol 1:86–93.

Collins D, Holmes C, Peters T, Evans A (1999): ANIMAL: automated nonlinear image matching and anatomical labeling. In: Toga AW, editor. Brain warping. San Diego: Academic Press. p 133–142.

Corbin JG, Nery S, Fishell G (2001): Telencephalic cells take a tangent: non-radial migration in the mammalian forebrain. Nat Neurosci 4(Suppl):1177–1182.

Fischl B, Sereno MI, Tootell RB, Dale AM (1999): High-resolution intersubject averaging and a coordinate system for the cortical surface. Hum Brain Mapp 8:272–284.

Fox PT (1995): Spatial normalization: origins, objective, applications, and alternatives. Hum Brain Mapp 3:161–164.

Fox PT, Raichle ME (1984): Stimulus rate dependence of regional cerebral blood flow in human striate cortex, demonstrated by positron emission tomography. J Neurophysiol 51:1109–1120.

Fox PT, Perlmutter JS, Raichle ME (1985): A stereotactic method of anatomical localization for positron emission tomography. J Comput Assist Tomogr 9:141–153.

Fox PT, Mintun MA, Reiman EM, Raichle ME (1988): Enhanced detection of focal brain responses using inter-subject averaging and change-distribution analysis of subtracted PET images. J Cereb Blood Flow Metab 8:642–653.

Galaburda AM, Sanides F (1980): Cytoarchitectonic organization of the human auditory cortex. J Comp Neurol 190:597–610.

Galaburda AM, Rosen GD, Sherman GF (1990): Individual variability in cortical organization: its relationship to brain laterality and implications to function. Neuropsychologia 28:529–546.

Gazzaniga MS (2000): Regional differences in cortical organization. Science 289:1887–1888.

Geschwind N, Galaburda AM (1985): Cerebral lateralization: biological mechanisms, associations, and pathology. I. A hypothesis and a program for research. Arch Neurol 42:428–459.

Goldman-Rakic PS (1980): Morphological consequences of prenatal injury to the primate brain. Prog Brain Res 53:3–19.

Green RL, Hutsler JJ, Loftus WC, Tramo MJ, Thomas CE, Silberfarb AW, Nordgren RE, Nordgren RA, Gazzaniga MS (1999): The caudal infrasylvian surface in dyslexia: novel magnetic resonance imaging-based findings. Neurology 53:974–981.

Habib M, Robichon F, Levrier O, Khalil R, Salamon G (1995): Diverging asymmetries of temporo-parietal cortical areas: a reappraisal of Geschwind/Galaburda theory. Brain Lang 48:238–258.

Hasnain MK, Fox PT, Woldorff MG (1998): Intersubject variability of functional areas in the human visual cortex. Hum Brain Mapp 6:301–315.

Hasnain MK, Fox PT, Woldorff MG (2001): Structure-function spatial covariance in the human visual cortex. Cereb Cortex 11:702–716.

Herscovitch P, Markham J, Raichle ME (1983): Brain blood flow measured with intravenous $H_2{}^{15}O$. I. Theory and error analysis. J Nucl Med 24:782–789.

Horton JC, Hoyt WF (1991): Quadrantic visual field defects: a hallmark of lesions in the extrastriate (V2/V3) cortex. Brain 114: 1703–1718.

Kochunov P, Lancaster J, Fox PT (1999): Accurate high-speed spatial normalization using an Octree method. Neuroimage 10:724–737.

Kochunov P, Lancaster JL, Thompson P, Boyer A, Hardies J, Fox PT (2000): Evaluation of Octree regional spatial normalization method for regional anatomical matching. Hum Brain Mapp 11:193–206.

Kochunov P, Hasnain M, Lancaster J, Grabowski T, Fox P (2003): Improvement in variability of the horizontal meridian of the primary visual area following high-resolution spatial normalization. Hum Brain Mapp 18:123–134.

Lancaster JL, Glass TG, Lankipalli BR, Downs JH, Mayberg H, Fox PT (1995): A modality-independent approach to spatial normalization of tomographic images of the human brain. Hum Brain Mapp 3:209–223.

Lancaster JL, Fox PT, Downs H, Nickerson DS, Hander TA, El Mallah M, Kochunov PV, Zamarripa F (1999): Global spatial normalization of the human brain using convex hulls. J Nucl Med 40:942–955.

LeMay M (1977): Asymmetries of the skull and handedness. J Neurol Sci 32:243–253.

Lohmann G, Cramon DYV, Steinmetz H (1999): Sulcal variability of twins. Cereb Cortex 9:754–763.

Ono M, Kubik S, Abernathy CD (1990): Atlas of the cerebral sulci. Stuttgart: Thieme.

Raichle ME, Martin WRW, Herscovitch P, Mintun MA, Markham J (1983): Brain blood flow measured with intravenous H_2 ^{15}O. II. Implementation and validation. J Nucl Med 24:790–798.

Rakic P (1990): Principles of neural cell migration. Experientia 46: 882–891.

Richman DP, Stewart RM, Hutchinson JW, Caviness VS Jr (1975): Mechanical model of brain convolutional development. Science 189:18–21.

Rosen GD (1996): Cellular, morphometric, ontogenetic and connectional substrates of anatomical asymmetry. Neurosci Biobehav Rev 20:607–615.

Savel'ev SV (1989): Mechanisms of embryonal formation of fissura calcarina in the human brain. Dokl Akad Nauk SSSR 309:204–207.

Scheibel AM (1984): A dendritic correlate of human speech. In: Geschwind N, Galaburda AM, editors. Cerebral dominance: the biological foundations. Cambridge, MA: Harvard University Press. p 43–52.

Schwartz ML, Rakic P, Goldman-Rakic PS (1991): Early phenotype expression of cortical neurons: evidence that a subclass of migrating neurons have callosal axons. Proc Natl Acad Sci U S A 88:1354–1358.

Sereno MI, Dale AM, Reppas JB, Kwong KK, Belliveau JW, Brady TJ, Rosen BR, Tootell RB (1995): Borders of multiple visual areas in humans revealed by functional magnetic resonance imaging. Science 268:889–893.

Smart IHM, McSherry GM (1986): Gyrus formation in the cerebral cortex of the ferret. II. Description of the internal histological changes. J Anat 147:27–43.

Talairach J and Tournoux P (1988): Co-planar stereotaxic atlas of the human brain. Stuttgart: Thieme.

Tramo MJ, Loftus WC, Thomas CE, Gazzaniga MS (1995): Surface area of human cerebral cortex and its gross morphological subdivisions: in vivo measurements in monozygotic twins suggest differential hemisphere effects of genetic factors. J Cogn Neurosci 7:292–301.

Van Essen DC (1997): A tension-based theory of morphogenesis and compact wiring in the central nervous system. Nature 385:313–318.

Welker W (1990): Why does cerebral cortex fissure and fold? A review of determinants of gyri and sulci. In: Jones EG, Peters A, editors. Cerebral cortex, vol. 8B. New York: Plenum. p 3–136.

Woods RP, Mazziota JC, Cherry SR (1993): MRI-PET registration with automated algorithm. J Comp Assist Tomogr 17:536–546.

Woods RP, Grafton ST, Watson JD, Sicotte NL, Mazziotta JC (1998): Automated image registration. II. Intersubject validation of linear and nonlinear models. J Comp Assist Tomogr 22:153–165.